LETTERS

Climate-driven trends in contemporary ocean productivity

Michael J. Behrenfeld[1], Robert T. O'Malley[1], David A. Siegel[3], Charles R. McClain[4], Jorge L. Sarmiento[5], Gene C. Feldman[4], Allen J. Milligan[1], Paul G. Falkowski[6], Ricardo M. Letelier[2] & Emmanuel S. Boss[7]

Contributing roughly half of the biosphere's net primary production (NPP)[1,2], photosynthesis by oceanic phytoplankton is a vital link in the cycling of carbon between living and inorganic stocks. Each day, more than a hundred million tons of carbon in the form of CO_2 are fixed into organic material by these ubiquitous, microscopic plants of the upper ocean, and each day a similar amount of organic carbon is transferred into marine ecosystems by sinking and grazing. The distribution of phytoplankton biomass and NPP is defined by the availability of light and nutrients (nitrogen, phosphate, iron). These growth-limiting factors are in turn regulated by physical processes of ocean circulation, mixed-layer dynamics, upwelling, atmospheric dust deposition, and the solar cycle. Satellite measurements of ocean colour provide a means of quantifying ocean productivity on a global scale and linking its variability to environmental factors. Here we describe global ocean NPP changes detected from space over the past decade. The period is dominated by an initial increase in NPP of 1,930 teragrams of carbon a year ($Tg\,C\,yr^{-1}$), followed by a prolonged decrease averaging 190 $Tg\,C\,yr^{-1}$. These trends are driven by changes occurring in the expansive stratified low-latitude oceans and are tightly coupled to coincident climate variability. This link between the physical environment and ocean biology functions through changes in upper-ocean temperature and stratification, which influence the availability of nutrients for phytoplankton growth. The observed reductions in ocean productivity during the recent post-1999 warming period provide insight on how future climate change can alter marine food webs.

Interannual changes in phytoplankton abundance are small relative to total standing stocks and require accurate, long-term measurements to detect. The first satellite sensor to have this capability is the Sea-viewing Wide Field-of-View Sensor (SeaWiFS) and so far it is the only ocean colour sensor to have lunar-viewing calibration capabilities[3]. These measurements allow SeaWiFS to achieve water-leaving radiance biases across the SeaWiFS visible bands (412–555 nm) of less than 4% when compared to field open-ocean observations[4]. The central biological variable derived from these measurements is upper-ocean chlorophyll concentration, which can be used to estimate phytoplankton standing stocks and productivity (Fig. 1a) throughout the photic zone[5].

Global, depth-integrated chlorophyll biomass (ΣChl) for the 1997 to 2006 SeaWiFS record varied from 4.2 to 5.0 Tg ($Tg = 10^{12}$ g). Monthly anomalies in global ΣChl for this period reveal two highly significant ($P < 0.0001$) trends (green line in Fig. 1b). The initial 0.3 Tg rise in ΣChl corresponds to the 1997 to 1999 El Niño to La Niña transition[2]. Since 1999, global chlorophyll concentrations dropped on average 0.01 Tg per year, with several secondary features that ended in a 2005 to 2006 rise (Fig. 1b). The two primary trends in global ΣChl are driven by changes occurring in the permanently stratified regions of the ocean (grey circles in Fig. 1b). These regions have annual average sea surface temperatures (SSTs) over 15 °C (black lines in Fig. 1a) and represent 74% of the global ice-free ocean. Cooler, seasonal seas also experienced local variability during the SeaWiFS period, but when integrated spatially they exhibit no significant overall trend ($P > 0.5$) (Supplementary Fig. 1).

The entire phytoplankton biomass of the global oceans is consumed every two to six days[6]. This rapid turnover implies that variability in ΣChl (Fig. 1b) corresponds to far more substantial changes in NPP. One of the most commonly used models for estimating NPP from satellite chlorophyll data is the Vertically Generalized Production Model (VGPM)[6]. The VGPM gives global NPP estimates for the SeaWiFS record that vary strongly with season and range from 3.8 to 4.6×10^{15} g of C per month. Monthly anomalies in this important carbon flux again reveal clear ($P < 0.0001$) temporal trends beginning with an El Niño/La Niña-driven 262 Tg increase in NPP between 1997 and 1999, followed by a 197 Tg decrease to 2004, and finally a modest increase during 2005 (green line in Fig. 1c). These prominent NPP trends are again traceable to changes in the permanently stratified oceans (grey circles in Fig. 1c), are highly correlated ($r^2 = 0.93$) with changes in ΣChl (Fig. 1b), and remain when NPP is reassessed using alternative productivity models (Supplementary Fig. 2).

Perhaps the most challenging aspect of understanding variability in biological processes is associating detected changes with the environmental forcings responsible. Important climate variables linked to ocean circulation and productivity are sea-level pressure, surface winds, SST, surface air temperature, and cloudiness. These physical factors have been combined into a Multivariate ENSO Index (MEI) for evaluating the strength of El Niño/Southern Oscillation cycles[7,8]. Strong El Niño/Southern Oscillation events have major impacts on phytoplankton, fisheries, marine birds and mammals[2,9–12] and are striking examples of climatic influences on ocean biology. Importantly, the MEI does not distinguish between natural and anthropogenic changes in climate forcing, but instead provides an integrated index of climate conditions for comparison with observed changes in ocean productivity.

We find a clear, strong correspondence between MEI variability and SeaWiFS-based anomalies in NPP ($r^2 = 0.77$, $P < 0.005$) (Fig. 2a) and ΣChl (Supplementary Fig. 3). An increase in the MEI (that is, warmer conditions) results in a decrease in NPP and ΣChl, and vice versa. This relationship emphasizes the pre-eminent role of climate

[1]Department of Botany and Plant Pathology, 2082 Cordley Hall, and [2]College of Oceanographic and Atmospheric Sciences, Oregon State University, Corvallis, Oregon 97331, USA. [3]Institute for Computational Earth System Science and Department of Geography, University of California, Santa Barbara, Santa Barbara, California 93106-3060, USA. [4]NASA Goddard Space Flight Center, Greenbelt, Maryland 20771, USA. [5]Atmospheric and Oceanic Sciences Program, Princeton University, PO Box CN710, Princeton, New Jersey 08544, USA. [6]Environmental Biophysics and Molecular Ecology Program, Institute of Marine and Coastal Sciences and Department of Geological Sciences, Rutgers University 71 Dudley Rd, New Brunswick, New Jersey 08901, USA. [7]School of Marine Sciences, 209 Libby Hall, University of Maine, Orono, Maine 04469-5741, USA.

variability on ocean productivity trends. The observed physical–biological coupling between NPP and the MEI (Fig. 2a) functions through an effect of climate on water column stratification. Climatic changes that allow surface warming cause an increase in the density contrast between the surface layer and underlying nutrient-rich waters. For the global stratified oceans, the density difference between the surface and a depth of 200 m provides a useful measure of stratification. Monthly anomalies in this stratification index exhibit similar trends as the MEI for the SeaWiFS period (Fig. 2b). Importantly, enhanced stratification suppresses nutrient exchange through vertical mixing. Conversely, surface cooling favours elevated vertical exchange. Phytoplankton in the ocean's upper layer (that is, the populations observed from space) rely on vertical nutrient transport to sustain productivity, so intensified stratification during a rising MEI period (Fig. 2b) is accompanied closely by decreasing NPP (Fig. 2b) ($r^2 = 0.73$, $P < 0.005$).

The MEI captures global-scale trends in climate forcings on surface ocean growth conditions for phytoplankton (Fig. 2). However, while an increasing MEI corresponds to an overall warming period, at the regional scale both warming and cooling events are found. These regional changes are registered in satellite SST data and are well illustrated by the 1999 to 2004 period of increasing MEI. Comparison of SST changes (Fig. 3a) and modelled NPP changes (Fig. 3b) for this period reveals the anticipated inverse relationship of increasing temperatures coupled to decreasing production (Fig. 3c). Quantitatively, over 74% of the global oceans with SST changes exceeding $\pm 0.15\,^{\circ}C$ between 1999 and 2004 exhibited an inverse relationship between temperature and NPP changes (Fig. 3c). A consistent relationship is likewise observed between SST and ΣChl (Supplementary Fig. 4).

Our results clearly link ΣChl and NPP changes to SST, stratification and climate variations and provide an opportunity for comparison with simulated ocean responses to a warming climate. Atmosphere–ocean general circulation models coupled to ocean ecosystem models are essential tools for understanding global carbon cycle–climate feedbacks. When forced by rising atmospheric CO_2 concentrations, these prognostic models consistently yield increased SSTs and net decreases in stratified ocean NPP[13–16], consistent with observed changes in NPP during the 1999 to 2004 period of rising MEI (Fig. 2a). Also consistent with our results, model-simulated NPP changes are largely due to intensified water-column stratification and are not uniformly distributed across the stratified oceans[13–16]. A warming climate in atmosphere–ocean general circulation models is also generally associated with increased NPP at higher latitudes, owing to improved mixed-layer light conditions and extended growing seasons[14–16]. For our relatively brief observational record, this anticipated net increase in high-latitude NPP was not observed, although NPP changes were found regionally (Fig. 3b).

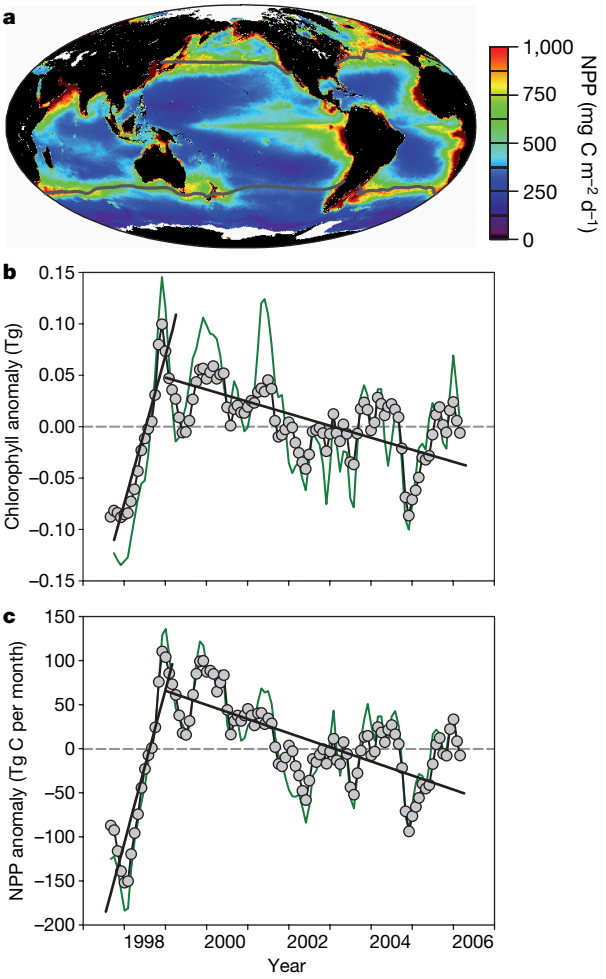

Figure 1 | Distribution and trends in global ocean phytoplankton productivity (NPP) and chlorophyll standing stocks. **a**, Annual average NPP showing high values where surface nutrients are elevated. Low-latitude, permanently stratified waters with annual average surface temperatures over 15 °C are delineated by black contour lines. **b**, Anomalies in globally integrated water-column chlorophyll concentrations (green line) are dominated by changes occurring in permanently stratified ocean regions (grey circles and black line). **c**, Anomalies in global NPP (green line) are likewise driven by changes in the permanently stratified oceans (grey circles and black line). Trend lines in **b** and **c** are least-squares fits to pre-1999 and post-1999 data.

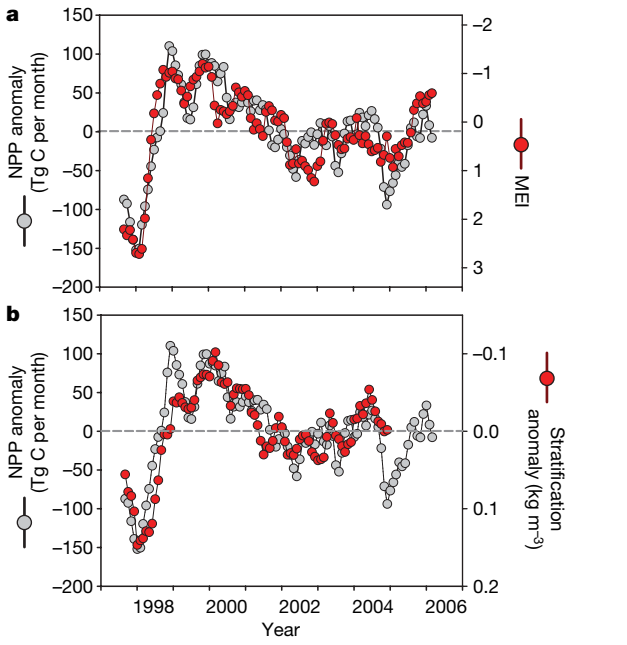

Figure 2 | Ocean productivity is closely coupled to climate variability. **a**, NPP anomalies in the permanently stratified oceans (grey symbols, left axis) are highly correlated ($r^2 = 0.77$) with the MEI of climate variability (red symbols, right axis). NPP data are from Fig. 1c. **b**, Changes in ocean stratification (red symbols, right axis) link climate variability to ocean biology, and are well correlated ($r^2 = 0.73$) with NPP anomalies (grey symbols, left axis) in ocean regions with annual average surface temperatures over 15 °C. Stratification strength was assessed as the density differences between the surface and a depth of 200 m using SODA data (see Methods). Publicly accessible SODA data are available only to the end of 2004. Note that the MEI and stratification axes (right) increase from top to bottom.

Establishing relationships between ocean biology and climate relies heavily on the accuracy to which changes in ocean ecosystems can be detected[3]. The unique operational characteristics of SeaWiFS have enabled detection of the global ocean trends reported here. Unfortunately, the SeaWiFS sensor is well beyond its design lifetime and no currently scheduled ocean-colour missions will have equal capabilities. SeaWiFS also represents an immature state of ocean-colour remote sensing. Modelling studies suggest that shifts in ecosystem structure from climate variations may be as or more important than the alterations in bulk integrated properties reported here[13]. Susceptible ecosystem characteristics include shifts in taxonomic composition[13], physiological status[17], and light absorption by coloured dissolved organic material[18]. Resolving these properties and their changes over time will require improved accuracies and significant expansions in the spectral range and resolution of future remote-sensing measurements.

Climate effects on ocean biology are documented here for nearly a decade of satellite ocean colour measurements. The compelling correspondence found between NPP changes and the MEI (Fig. 2a) suggests that this integrated index of climate variability, which extends back to 1950 (refs 6, 7), may provide a first-order proxy for variations in photosynthetic carbon fixation in the oceans for the period predating satellite ocean-colour measurements. It is also clear from the current analysis that surface warming in the permanently stratified ocean regions is accompanied by reductions in productivity. The index used here (MEI) to relate climate variability to NPP trends does not distinguish natural from anthropogenic contributions, but observational and modelling efforts indicate that recent changes in SST are strongly influenced by anthropogenic forcing[19–22]. These observations imply that the potential transition to permanent El Niño conditions in a warmer climate state[23] would lead to lower and redistributed ocean carbon fixation relative to typical contemporary conditions. Such changes will inevitably alter the magnitude and distribution of global ocean net air–sea CO_2 exchange[15,24,25], fishery yields[9,12,26], and dominant basin-scale biological regimes[12].

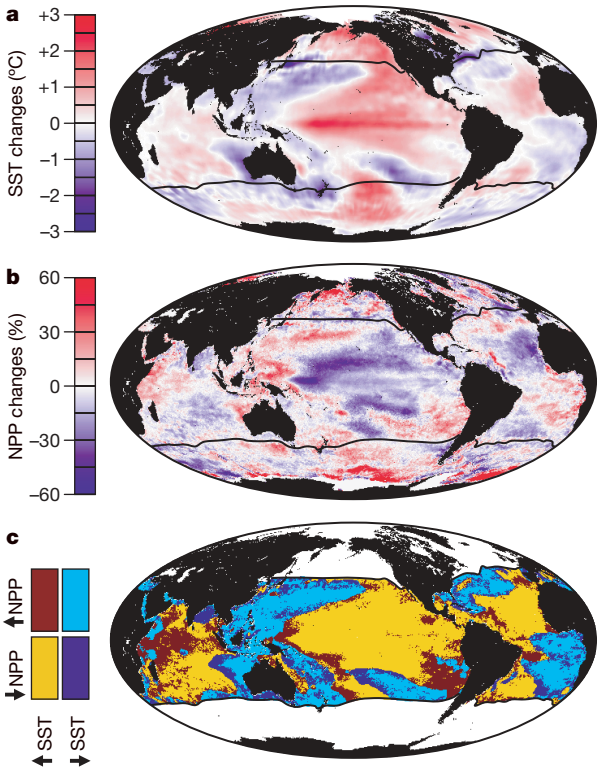

Figure 3 | Climate controls on ocean productivity cause NPP to vary inversely with changes in SST. Global changes in annual average SST (**a**) and NPP (**b**) for the 1999 to 2004 warming period (Fig. 2). **c**, For 74% of the permanently stratified oceans (that is, regions between black contour lines), NPP and SST changes were inversely related. Yellow, increase in SST, decrease in NPP. Light blue, decrease in SST, increase in NPP. Dark blue, decreases in SST and NPP. Dark red, increases in SST and NPP. A similar inverse relationship is observed between SST and chlorophyll changes. (See Supplementary Fig. 4 for additional information.)

METHODS

Ocean NPP was calculated with the VGPM using monthly 1,080 × 2,160 pixel resolution (that is, 18 km spacing at the Equator) OC4-v4 chlorophyll algorithm products from SeaWiFS reprocessed version 5.1 data (http://oceancolor.gsfc.nasa.gov). Comparison of this data with ~1,400 *in situ* match-up surface chlorophyll data yields a median difference of 33%, which is comparable to measurement uncertainties in the field. ΣChl was calculated from the satellite chlorophyll data using relationships described in ref. 5, which are based on 3,806 *in situ* chlorophyll profiles and account for subsurface chlorophyll features. The VGPM describes light-dependent changes in water-column NPP using a relationship based on 1,698 field productivity measurements[6] and SeaWiFS cloud-corrected photosynthetically active radiation data (http://oceancolor.gsfc.nasa.gov). The standard VGPM describes photosynthetic efficiencies using a polynomial function that increases with temperature below 20 °C and decreases above 20 °C.

Ocean NPP was additionally calculated using two alternative models, with results demonstrating the robust nature of the primary temporal trends described here (Supplementary Fig. 2). MEI data were from http://www.cdc.noaa.gov/people/klaus.wolter/MEI. Stratification anomalies were calculated from Simple Ocean Data Assimilation (SODA) (http://www.atmos.umd.edu/~ocean) monthly global density data, which assimilate available field observations. AVHRR SST data were from http://podaac-www.jpl.nasa.gov/sst. Deseasonalized chlorophyll, NPP, and stratification anomalies were calculated by subtracting from each monthly value the corresponding monthly average for the entire time series. Reported statistics for relationships between NPP anomalies and MEI and stratification anomalies account for auto-correlation effects inherent in comparisons between time-series data sets.

Received 18 August; accepted 6 October 2006.

1. Field, C. B., Behrenfeld, M. J., Randerson, J. T. & Falkowski, P. G. Primary production of the biosphere: Integrating terrestrial and oceanic components. *Science* **281,** 237–240 (1998).
2. Behrenfeld, M. J. *et al.* Biospheric primary production during an ENSO transition. *Science* **291,** 2594–2597 (2001).
3. McClain, C. R., Feldman, G. C. & Hooker, S. B. An overview of the SeaWiFS project and strategies for producing a climate research quality global ocean bio-optical time series. *Deep-Sea Res. II* **51,** 5–42 (2004).
4. Bailey, S. W. & Werdell, P. J. A multi-sensor approach for the on-orbit validation of ocean color satellite data products. *Remote Sens. Environ.* **102,** 12–23 (2006).
5. Morel, A. & Berthon, J-F. Surface pigments, algal biomass profiles, and potential production of the euphotic layer: relationships reinvestigated in view of remote-sensing applications. *Limnol. Oceanogr.* **34,** 1545–1562 (1989).
6. Behrenfeld, M. J. & Falkowski, P. G. Photosynthetic rates derived from satellite-based chlorophyll concentration. *Limnol. Oceanogr.* **42,** 1–20 (1997).
7. Wolter, K. The Southern Oscillation in surface circulation and climate over the tropical Atlantic, Eastern Pacific, and Indian Oceans as captured by cluster analysis. *J. Clim. Appl. Meteorol.* **26,** 540–558 (1987).
8. Wolter, K. & Timlin, M. S. Monitoring ENSO in COADS with a seasonally adjusted principal component index. In *Proc. 17th Climate Diagnostics Workshop (Norman, Oklahoma)* 52–57 (NOAA/N MC/CAC, NSSL, Oklahoma Climate Survey, CIMMS and the School of Meteorology, Univ. Oklahoma, 1993).
9. Barber, R. T. & Chavez, F. P. Biological consequences of El Niño. *Science* **222,** 1203–1210 (1983).
10. Chavez, F. P. *et al.* Biological and chemical response of the equatorial Pacific ocean to the 1997–98 El Niño. *Science* **286,** 2126–2131 (1999).
11. Turk, D., McPhaden, M. J., Lewis, M. R. & Busalacchi, A. J. Remotely-sensed biological production in the Tropical Pacific during 1992–1999. *Science* **293,** 471–474 (2001).
12. Chavez, F. P., Ryan, J., Lluch-Cota, S. E. & Niquen, M. C. From anchovies to sardines and back: Multidecadal change in the Pacific ocean. *Science* **299,** 217–221 (2003).
13. Boyd, P. W. & Doney, S. C. Modelling regional responses by marine pelagic ecosystems to global climate change. *Geophys. Res. Lett.* **29,** 1806, doi:10.1029/2001GL014130 (2002).
14. Bopp, L. *et al.* Potential impact of climate change on marine export production. *Glob. Biogeochem. Cycles* **15,** 81–99 (2001).
15. Le Quéré, C., Aumont, O., Monfray, P. & Orr, J. Propagation of climatic events on ocean stratification, marine biology, and CO2: Case studies over the

1979–1999 period. *J. Geophys. Res.* **108,** 3375, doi:10.1029/2001JC000920 (2003).
16. Sarmiento, J. L. *et al.* Response of ocean ecosystems to climate warming. *Glob. Biogeochem. Cycles* **18,** GB3003, doi:10.1029/2003GB002134 (2004).
17. Behrenfeld, M. J., Boss, E., Siegel, D. A. & Shea, D. M. Carbon-based ocean productivity and phytoplankton physiology from space. *Glob. Biogeochem. Cycles* **19,** GB1006, doi:10.1029/2004GB002299 (2005).
18. Siegel, D. A., Maritorena, S., Nelson, N. B. & Behrenfeld, M. J. Independence and interdependences of global ocean optical properties viewed using satellite color imagery. *J. Geophys. Res.* **110,** C07011, doi:10.1029/2004JC002527 (2005).
19. Levitus, S., Antonov, J. I., Boyer, T. P. & Stephens, C. Warming of the world ocean. *Science* **287,** 2225–2229 (2000).
20. Barnett, T. P., Pierce, D. W. & Schnur, R. Detection of anthropogenic climate change in the world's oceans. *Science* **292,** 270–274 (2001).
21. Levitus, S. *et al.* Anthropogenic warming of Earth's climate system. *Science* **292,** 267–270 (2001).
22. Barnett, T. P. *et al.* Penetration of human-induced warming into the world's oceans. *Science* **309,** 284–287 (2005).
23. Wara, M. W., Ravelo, A. C. & DeLaney, M. L. Permanent El Niño-like conditions during the Pliocene warm period. *Science* **309,** 758–761 (2005).
24. Sarmiento, J. L., Hughes, T. M. C., Stouffer, R. J. & Manabe, S. Simulated response of the ocean carbon cycle to anthropogenic climate warming. *Nature* **393,** 245–249 (1998).
25. Laws, E. A., Falkowski, P. G., Smith, W. O. Jr & McCarthy, J. J. Temperature effects on export production in the open ocean. *Glob. Biogeochem. Cycles* **14,** 1231–1246 (2000).
26. Ware, D. M. & Thomson, R. E. Bottom-up ecosystem trophic dynamics determine fish production in the Northeast Pacific. *Science* **308,** 1280–1284 (2005).

Supplementary Information is linked to the online version of the paper at www.nature.com/nature.

Acknowledgements We thank the Ocean Biology Processing Group at the Goddard Space Flight Center, Greenbelt, Maryland for their diligence in providing the highest quality ocean colour products possible and the NASA Ocean Biology and Biogeochemistry Program for support.

Author Information Reprints and permissions information is available at www.nature.com/reprints. The authors declare no competing financial interests. Correspondence and requests for materials should be addressed to M.J.B. (mjb@science.oregonstate.edu).

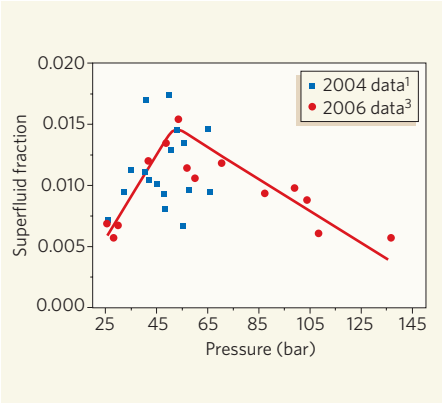

Figure 1 | Supersolid component. The superfluid fraction in crystalline ^{4}He in the low-temperature limit, as a function of pressure, from Kim and Chan's data[1,3]. Crystals grown at constant pressure and temperature (2006 data)[3] show somewhat less variation in the supersolid fraction than do those grown at constant volume (2004 data)[1]. The fraction also does not decrease sharply with increasing pressure, as would be expected if the phenomenon were the result of quantum-mechanical exchange processes in a perfect crystal. The solid line is a guide to the eye.

component should have flowed immediately through the fine pores, but no superflow was observed. This year, however, Sasaki and colleagues[6] have observed bulk superflow. Again, it is not seen in all samples, but only in those that have a large, observable boundary between two grains (regions of distinct crystallographic orientations) extending across the sample. Superflow seems to occur along, or close to, these grain boundaries.

To understand the significance of these results[3–6], one must first know that there are two prevalent pictures of superfluidity. The first of these focuses on the quantum-mechanical exchange, or tunnelling, of atoms between lattice sites. At low temperature, the de Broglie wavelength of ^{4}He atoms — a quantum-mechanical measure of a particle's extent in space —is long and covers many sites. A long wavelength enables long-range exchange of atoms between lattice sites. If the exchanges extend right across the sample, superfluidity occurs.

The second picture is based on the phenomenon of Bose–Einstein condensation. Any number of the particles known as bosons, which possess integer spin, may occupy a single quantum state. If, at low temperature, a macroscopic fraction of bosons condenses into a single state, a long-range coherence is brought to the system that makes superfluidity possible. In liquid ^{4}He, the classic superfluid, Bose–Einstein condensation is known to occur below the critical temperature for superfluidity in this system, 2.17 K. As the temperature approaches absolute zero — where ρ_s is 100% — the condensed fraction is around 7%.

Early theoretical discussions[8–10] of possible superflow in solid ^{4}He involved quantum tunnelling through ground-state vacancies (these are lattice sites that are vacant at absolute zero), as well as Bose–Einstein condensation and quantum exchanges within the lattice. The predicted[10] superfluid fraction within the lattice was of the order 0.01%. Unfortunately, however, ground-state vacancies have not been observed in solid ^{4}He. Thermally activated vacancies are found — but at temperatures above T_C that are irrelevant to the establishment of superfluidity. Recent calculations[11] also find that individual vacancies are not stable in the ground state of crystalline ^{4}He. The vacancies instead coalesce or migrate to a surface; this is the mechanism by which thermal vacancies leave a classical crystal when it is cooled.

Calculations have also shown that there is no long-range coherence, and so no Bose–Einstein condensation, in a perfect crystal of ^{4}He, essentially because condensation requires double occupancy of a lattice site[12,13]. In real crystals, the condensate fraction is observed in neutron-scattering experiments[14] to be $0.2 \pm 0.6\%$ — that is, compatible with zero — at a temperature of 0.08 K. Similarly, long-range quantum exchanges within crystalline ^{4}He are too infrequent to explain the high ρ_s observed[15]. As seen in solid ^{3}He, quantum exchange rates decrease dramatically as a solid is compressed under pressure. If the superfluid fraction arises from exchanges of particles between lattice sites, ρ_s should decrease by orders of magnitude under increasing pressure. But Kim and Chan[3] find ρ_s to be largely independent of pressure (Fig. 1). Superflow in crystalline ^{4}He thus does not seem to be a phenomenon of the perfect bulk solid[11–13,15], or to involve individual point defects (vacancies) that are in equilibrium at absolute zero.

Given the recently discovered dependence of ρ_s on sample annealing[3–5], and the correlation of superflow with grain boundaries[6], supersolidity seems to hinge on macroscopic, long-range defects such as grain boundaries or amorphous channels in the helium crystal. But at the same time, a superfluid density of the same magnitude is observed[1] in helium confined in a nanoporous medium such as Vycor. It is difficult to imagine that extended defects could be the same in helium thus confined and in bulk helium. The situation is far from clear: revealing the secrets of this latest superfluid is very much a work in progress. ■

Henry R. Glyde is in the Department of Physics and Astronomy, University of Delaware, Newark, Delaware 19716, USA.
e-mail: glyde@udel.edu

1. Kim, E. & Chan, M. H. W. *Nature* **427,** 225–227 (2004).
2. Kim, E. & Chan, M. H. W. *Science* **305,** 1941–1944 (2004).
3. Kim, E. & Chan, M. H. W. *Phys. Rev. Lett.* **97,** 115302 (2006).
4. Rittner, A. S. C. & Reppy, J. D. *Phys. Rev. Lett.* **97,** 165301 (2006).
5. Shirahama, K., Kondo, M., Takada, S. & Shibayama, Y. *Am. Phys. Soc. March Meet.* Abstr. G41.00007 (2006).
6. Sasaki, S., Ishiguro, R., Caupin, F., Maris, H. J. & Balibar, S. *Science* **313,** 1098–1100 (2006).
7. Day, J. & Beamish, J. *Phys. Rev. Lett.* **95,** 105304 (2006).
8. Andreev, A. F. & Lifshitz, I. M. *Sov. Phys. JETP* **29,** 1107–1113 (1969).
9. Chester, G. V. *Phys. Rev. A* **2,** 256–258 (1970).
10. Leggett, A. J. *Phys. Rev. Lett.* **25,** 1543–1546 (1970).
11. Boninsegni, M. *Phys. Rev. Lett.* **97,** 080401 (2006).
12. Boninsegni, M., Prokof'ev, N. & Svistunov, B. *Phys. Rev. Lett.* **96,** 105301 (2006).
13. Clark, B. K. & Ceperley, D. M. *Phys. Rev. Lett.* **96,** 105302 (2006).
14. Diallo, S. O., Pearce, J. V., Taylor, J. W., Kirichek, O. & Glyde, H. R. *Quantum Fluids and Solids Symp.* Kyoto, August 2006 (in the press).
15. Ceperley, D. M. & Bernu, B. *Phys. Rev. Lett.* **93,** 155303 (2004).

OCEANOGRAPHY

Plankton in a warmer world

Scott C. Doney

Satellite data show that phytoplankton biomass and growth generally decline as the oceans' surface waters warm up. Is this trend, seen over the past decade, a harbinger of the future for marine ecosystems?

Oranges in Florida, wildfires in Indonesia, plankton in the North Pacific — what links these seemingly disparate items is that they are all affected by year-to-year fluctuations in global-scale climate. On page 752 of this issue, Behrenfeld *et al.*[1] describe how such fluctuations, especially in temperature, are connected to the productivity of phytoplankton in the world's oceans. Their analyses are based on nearly a decade of satellite data, and for much of the oceans they find that recent warmer surface temperatures correspond to lower oceanic biomass and productivity. Behrenfeld *et al.* argue that these patterns arise because climate-induced changes in ocean circulation reduce the supply of nutrients needed for photosynthesis.

Small photosynthetic phytoplankton grow in the well-illuminated upper ocean, forming the base of the marine food web and supporting the fish stocks we harvest. They also form the basis of the biogeochemical cycling of carbon and many other elements in the sea. Phytoplankton growth depends on temperature and the availability of light and nutrients, including nitrogen, phosphorus, silicon and iron. Most of this nutrient supply to the surface ocean comes from the mixing and upwelling of cold, nutrient-rich

NATURE|Vol 444|7 December 2006

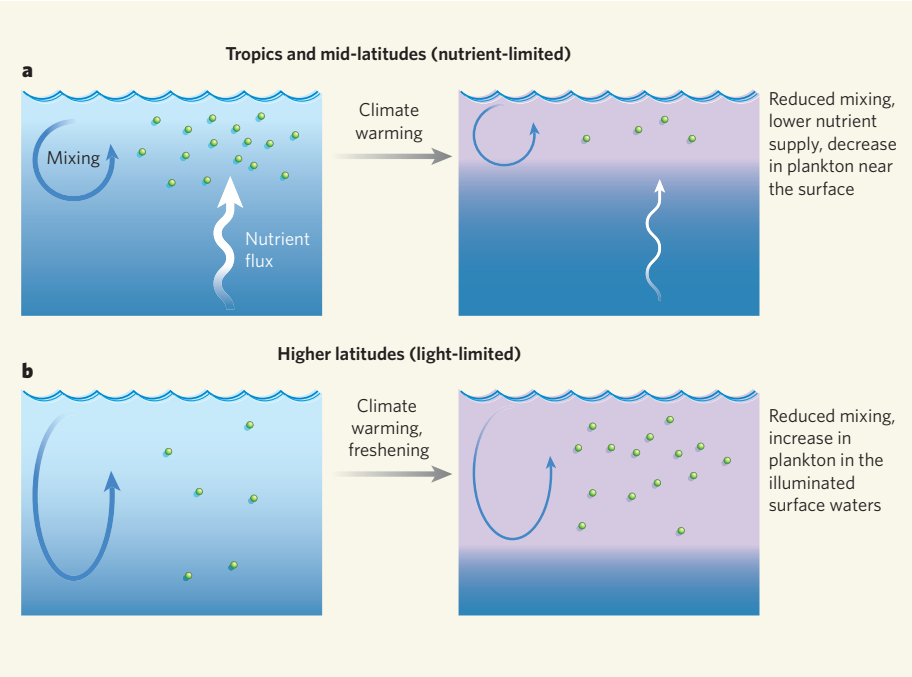

Figure 1 | Predicted phytoplankton response to increased temperature in ocean surface waters[1]. **a**, In the tropics and at mid-latitudes, phytoplankton are typically nutrient-limited, and satellite data tie reduced biological productivity to upper-ocean warming and reduced nutrient supply. **b**, At higher latitudes, the opposite biological response to future warming, and extra freshwater input, may occur. In these regions, phytoplankton are often light-limited; reduced mixing would keep plankton close to the surface where light levels are higher.

water from below, with an additional source of iron from mineral dust swept off the continental deserts. Phytoplankton biomass can vary by a factor of 100 in surface waters; its geographical distribution is determined largely by ocean circulation and upwelling, with the highest levels being found along the Equator, in temperate and polar latitudes, and along the western boundaries of continents.

Although the broad spatial patterns of phytoplankton biomass and productivity are well documented[2], large-scale temporal variations have only recently become quantifiable with the advent of satellite ocean-colour sensors[3]. The ocean is vast, and the limited number of research ships move at about the speed of a bicycle, too slow to map the ocean routinely on ocean-basin to global scales. By contrast, a satellite can observe the entire globe, at least the cloud-free areas, in a few days. Phytoplankton biomass and growth rates can be estimated remotely from space because chlorophyll, the main photosynthetic pigment in phytoplankton, absorbs blue and red sunlight more readily than green sunlight. Ocean-colour sensors measure, by wavelength band, the small fraction of sunlight scattered back to space from below the surface. The resulting surface-chlorophyll data can be combined with empirical relationships to estimate phytoplankton growth rates or net primary production[4].

Not that this procedure is straightforward: other constituents of sea water absorb light; many photons reaching the satellite sensor come from atmospheric aerosols or reflection at the water surface; and optical detectors on satellites degrade with time. But with careful calibration, high-quality, long-term records of ocean-colour data can be constructed for detecting climate-driven trends. The best such record at present is from GeoEye and from NASA's Sea-viewing Wide Field-of-view Sensor (SeaWiFS)[3], launched in 1997. In the SeaWiFS time series, global chlorophyll and productivity increase sharply during 1997–98 and then decline gradually to 2005.

Behrenfeld *et al.*[1] show that these trends closely follow changes in climate. The phytoplankton increase in 1997–98 matches a negative (cold) phase of the El Niño–Southern Oscillation (ENSO), and the subsequent slow drop occurred as the planet moved into an extended warm ENSO period. ENSO is a dominant mode of interannual climate variability, and involves large-scale reorganizations of atmosphere and ocean circulation that originate in the equatorial Pacific and extend across the globe. Decreases in productivity are equally well related to increases in sea surface temperatures and vertical temperature gradients in the upper ocean.

The climate–plankton link is found primarily in the tropics and mid-latitudes, where there is limited vertical mixing because the water column is stabilized by thermal stratification (that is, when light, warm waters overlie dense, cold waters). In these areas, the typically low levels of surface nutrients limit phytoplankton growth. Climate warming further inhibits mixing, reducing the upward nutrient supply and lowering productivity (Fig. 1a). At higher latitudes, phytoplankton are often light-limited because intense vertical mixing carries them hundreds of metres down into darkness where sunlight does not penetrate. In these regions, future warming and a greater influx of fresh water, mostly from increased precipitation and melting sea-ice, will contribute to reduced mixing that may actually increase productivity[5] (Fig. 1b).

The recent observed global surface warming (about 0.2 °C per decade) is expected to accelerate in coming decades as we continue to release excess carbon dioxide into the atmosphere. In fact, the planet may soon be warmer than at any time in the past million years[6]. Extrapolating the satellite observations into the future suggests that marine biological productivity in the tropics and mid-latitudes will decline substantially, in agreement with climate-model simulations[7–9]. In those simulations, the geographical boundaries that separate specific marine ecosystems (the ocean equivalents of forests, grasslands and so on) migrate towards the poles, and productivity increases at high latitudes because of surface warming, enhanced freshwater input and reduced deep mixing. Ecosystem dynamics are complex and nonlinear, however, and unexpected phenomena may arise as we push the planet into this unknown climate state. For example, oceanic fixation of atmospheric nitrogen into biologically available forms is concentrated in warm, nutrient-poor surface waters; under more stratified conditions, fixation might increase and enhance overall productivity[8,10].

Detecting the impact of climate change requires increased and more sophisticated monitoring of ocean biology and environmental change, both from space and with instruments in the water. Ideally, we need measures not only of such parameters as chlorophyll concentration and productivity, but also of plankton taxonomy (what is there?) and physiology (how healthy are they?). New remote-sensing technologies may help meet these challenges[11]. ■

Scott C. Doney is in the Marine Chemistry and Geochemistry Department, Woods Hole Oceanographic Institution, Woods Hole, Massachusetts 02543, USA.
e-mail: sdoney@whoi.edu

1. Behrenfeld, M. J. *et al. Nature* **444,** 752–755 (2006).
2. Longhurst, A. *Ecological Geography of the Sea* 2nd edn (Academic, New York, 2006).
3. McClain, C. R., Feldman, G. C. & Hooker, S. B. *Deep-Sea Res. II* **51,** 5–42 (2004).
4. Carr, M.-E. *et al. Deep-Sea Res. II* **53,** 741–770 (2006).
5. Polovina, J. J., Mitchum, G. T. & Evans, G. T. *Deep-Sea Res. I* **42,** 1701–1716 (1995).
6. Hansen, J. *et al. Proc. Natl Acad. Sci. USA* **103,** 14288–14293 (2006).
7. Bopp, L. *et al. Glob. Biogeochem. Cycles* **15,** 81–99 (2001).
8. Boyd, P. W. & Doney, S. C. *Geophys. Res. Lett.* **29,** 1806 (2002).
9. Sarmiento, J. L. *et al. Glob. Biogeochem. Cycles* **18,** GB3003; doi:10.1029/2003GB002134 (2004).
10. Karl, D. *et al. Nature* **388,** 533–538 (1997).
11. NASA OBB Advanced Planning Team *Plan for Earth's Living Ocean: The Unseen World to Set NASA's Ocean Biology and Biogeochemistry Agenda* (NASA, in the press).